Contributed paper

OPTO-ELECTRONICS REVIEW **12**(2), 187–192 (2004)

Modelling of dynamic performance of semiconductor lasers under subthreshold biasing

P. KREHLIK* and Ł. ŚLIWCZYŃSKI

Institute of Electronics, University of Mining and Metallurgy
30 Mickiewicza Ave., 30-059 Cracow, Poland

The problem of turn-on delay induced by the subthreshold bias of the semiconductor laser in the burst-mode fiber optic transmitters is discussed. An easy to use method of estimation of the turn-on delay is proposed and experimentally verified. The Simulink model of the laser is proposed, allowing to simulate the data pattern distortions in fiber optic communication systems. Presented considerations may be useful for high-speed burst-mode system designers.

Keywords: semiconductor laser, subthreshold biasing, burst-mode transmitters.

1. Introduction

The passive optical networks (PONs) [1–4] create new requirements for laser transmitters. In such a network (Fig. 1), an upstream traffic is organised in the form of time division multiple access (TDMA) where the number of transmitters send bursts of data (in prescribed time slots) to the same receiver. Thus, residual optical powers of inactive transmitters build up at the receiver input cause an undesirable pedestal in the optical signal, difficult to be dealt with in the receiver circuitry [5,6]. One of the proposed solutions is to eliminate the residual optical power by subthreshold laser biasing [3,7]. This allows the laser to be completely extinct, but on the other hand some dynamic distortions, caused by the laser turn-on delay, arise. The aim of this paper is to give the method of quantitative estimation of these distortions in various biasing and modulation conditions, basing on a few easy measurable laser parameters.

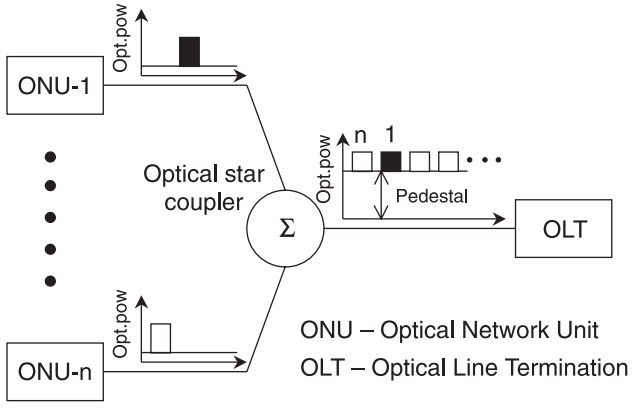

Fig. 1. Data upstream transmission in a typical PON.

2. Data pattern distortion under subthreshold laser biasing

When biased below threshold, the optical gain of semiconductor laser active region is insufficient for stimulated emission and output optical power is very low. To start lasing, the threshold carrier concentration should be reached in the laser active region. Thus, when the modulating current is applied to the subthreshold biased laser, some time must elapse to rise the carrier concentration to the threshold level. It is equivalent to the delay in laser optical power turn-on. This effect is illustrated on the plots shown in Fig. 2.

Initially, when the current flowing through the laser is below the threshold value ($I_B < I_{TH}$), some initial carrier concentration N_B is established, but no significant optical power is emitted. After applying the current pulse, the carrier concentration rises with a slope dependent on the carrier lifetime and the current step value. When the concen-

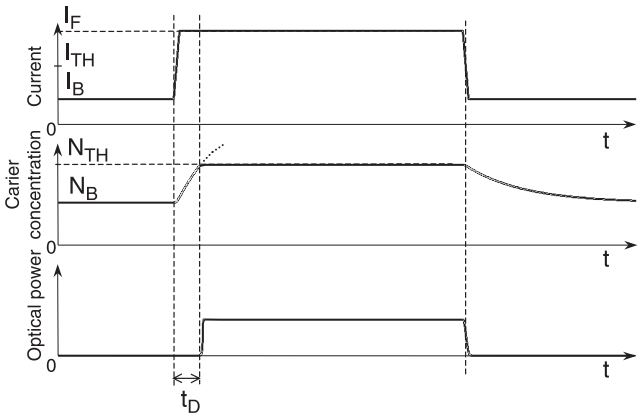

Fig. 2. Laser turn-on delay.

*e-mail: krehlik@uci.agh.edu.pl

tration reaches the threshold value N_{TH}, the lasing starts, and so the optical power appears after the turn-on delay t_D. Further increase in the carrier concentration (dotted line in Fig. 2) is eliminated because of the lasing process, so it becomes clamped to N_{TH} regardless to the current pulse amplitude [8,9]. Thus, when the current pulse finishes, the concentration drops below the threshold practically immediately, so no significant turn-off delay occurs. The difference between turn-on and turn-off behaviour leads to the pulse-width distortion.

Although there is no significant delay during optical signal turn-off, the carrier concentration diminishes relatively slowly, according to the carrier lifetime. When the next current pulse is applied, the optical response turn-on delay depends on the residual carrier concentration, what is sometimes referred as so-called patterning effect.

The turn-on dependence on the time interval from the previous pulse is illustrated in Fig. 3. The solid, dashed and dotted lines are used for different time intervals between two consecutive current pulses, relevant carrier concentration and optical power plots. It is seen that if the turn-off time is shortened, the residual carrier concentration stays significant and the turn-on delay is reduced.

When investigating the impact of the aforementioned dynamic distortions on the standard intensity modulation (IM) fibre optic data transmission system, it is convenient to analyse the data eye pattern. The comparison between ideal and distorted eye pattern is shown in Fig. 4. For subthreshold biased laser the rising edges of the optical signal are delayed, so the pulse-width is distorted, and the horizontal eye opening is reduced. Additionally, this delay is affected by the number of consecutive "zero" symbols transmitted prior to actual rising edge (i.e., the "zero" to "one" transition). This results in pattern dependent jitter, what disturbs the clock recovery circuitry in the receiver [1,10,11]. It should be mentioned that, for a given turn-on delay, the eye pattern degradation increases with a data bit rate, and so becomes a serious problem for nowadays transmitters operating at gigabit-per-second rates.

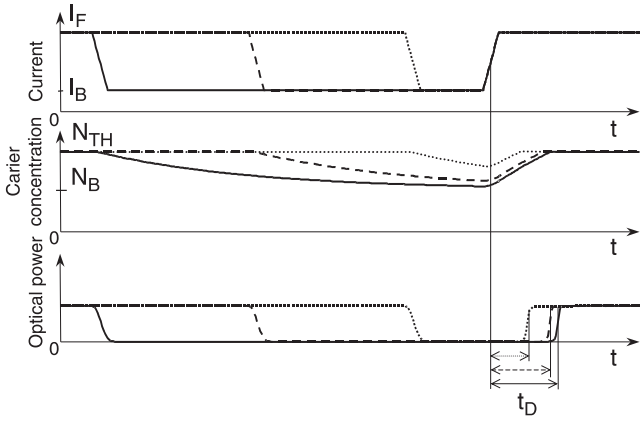

Fig. 3. Turn-on dependence on interval between current pulses.

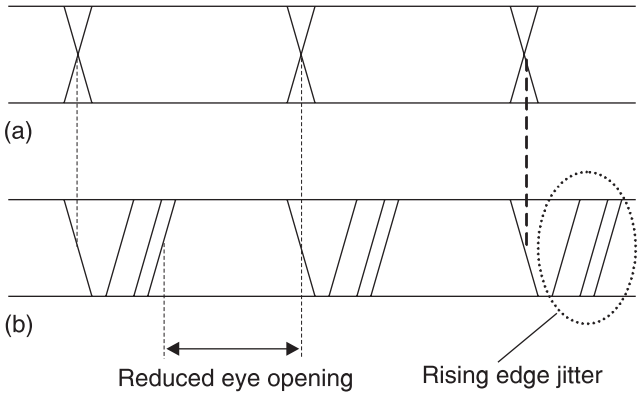

Fig. 4. Ideal (a) and distorted (b) data eye pattern.

3. Laser turn-on delay estimation

Although the turn-on delay effects are widely described in literature [3,7–9], there is lack of quantitative data and estimation methods useful for laser driver designers. Basically, the laser dynamics is completely described by the rate equations [8,9], but unfortunately they need a large set of difficult to obtain parameters [12,13] what make them practically useless for driver designers. In the following chapter, we propose the expression for the turn-on delay, basing on two easy measurable laser parameters.

Because the turn-on delay is determined by the up-to-threshold growth of carrier concentration, the simplified laser rate equation may be used for calculations. In the subthreshold regime (i.e., for $N < N_{TH}$) this equation can be expressed as [8]

$$\frac{dN}{dt} = \frac{\eta I}{qV} - R(N), \tag{1}$$

where N is the carrier concentration, η is the current injection efficiency, I is the supply current, V is the laser active volume, and $R(N)$ is the recombination rate. In general, $R(N)$ may be written as [8]

$$R(N) = AN + BN^2 + CN^3, \tag{2}$$

where A, B and C are the unimolecular, bimolecular, and Auger recombination coefficients, respectively. Restricting the considerations to the long-wavelength lasers (i.e., 1.3 μm and 1.55 μm), the coefficients A and B approximately may be assumed to be zero [8], and Eq. (1) may be rewritten as

$$\frac{dN}{dt} = \frac{\eta I}{qV} - CN^3. \tag{3}$$

Thus, assuming that during the pulse the current is constant and equals I_F, the turn-on delay is

$$t_D = \int_{N_I}^{N_{TH}} \frac{1}{\frac{\eta I_F}{qV} - CN^3} dN, \tag{4}$$

where N_I is the initial carrier concentration at the beginning of a driving current pulse.

Unfortunately, neither the threshold concentration nor some equation parameters are known for the driver designer. To overcome this problem we proposed to replace the carrier concentration by the equivalent steady-state laser current. Putting $dN/dt = 0$ into Eq. (3) it can be written

$$N = \left(\frac{\eta J}{qVC} \right)^{1/3}, \tag{5}$$

where J is the steady state current producing certain carrier concentration N.

Using Eq. (4), Eq. (3) can be rewritten as

$$\frac{dJ}{dt} = \frac{1}{c} J^{2/3} (I - J) \tag{6}$$

where

$$c = \frac{1}{3} \left(\frac{q^2 V^2}{\eta^2 C} \right)^{1/3}, \tag{7}$$

is the parameter which may be determined experimentally. Similarly to Eq. (4), the turn-on delay may be written as

$$t_D = c \int_{J_I}^{J_{TH}} \frac{J^{-2/3}}{I_F - J} dJ, \tag{8}$$

where J_{TH} is simply equal to the laser threshold current I_{TH} and J_I is the initial value of J which depends on the bias current and the time interval between the present and previous pulse. Its value may be find numerically from Eq. (6). However, when this time interval is long enough, i.e., the laser was in the steady state before the pulse beginning, J_I is equal to the bias current I_B. Thus, by measuring t_D for some particular values of I_B and I_F, the parameter c may be obtained from Eq. (8). It may be pointed out that only two laser parameters, i.e., the threshold current and c used in Eqs. (6) and (8) are sufficient to describe laser turn-on behaviour.

4. Simulation model

Basing on the above considerations, the dynamic performance of semiconductor lasers under subthreshold biasing may be modelled.

The basis of the model is nonlinear state Eq. (6). Additionally, it should be taken into account that accordingly to carrier concentration behaviour, the equivalent current J may increase only to the threshold value I_{TH}. When J arises to the threshold, the lasing starts and J is clamped, so $dJ/dt = 0$ should be used instead of Eq. (6). In this regime, an optical power appears and may be calculated as [1,8]

$$P = \varepsilon (I - I_{TH}), \tag{9}$$

where ε is the laser slope efficiency. When the driving current I falls below I_{TH}, optical power disappears, and J diminishes accordingly to Eq. (6).

The model described above was implemented as Simulink M-file S-function and is presented in Fig. 5. Some results obtained using this model will be shown in the next section.

5. Experimental results

To verify usefulness of the proposed turn-on delay estimation method, various long-wavelength (1.3 μm and 1.55 μm) communication lasers were examined, using a

```
function [sys,J0,str,ts] = lasmod(t,J,I,flag,Ith,c,eps)
% S-function parameters:
%   Ith  laser threshold current
%   c  equation (6) parameter
%   eps  laser slope efficiency

switch flag
    case 0                  % Initialization
        sys = [1,0,1,1,0,1,1];
        J0 = 1e-5           % initial cond.
        str = [ ];
        ts = [0,0];

    case 1                  % Derivatives
        if (J >= Ith & I > Ith)
            sys = 0;
        else
            sys = (J^2)^(1/3)*(I-J)/c;
end

    case 2                  % Discrete state update
        sys = [ ];

    case 3                  % Outputs
        if J <= Ith
            sys = 0;
        else
            sys = eps*(I-Ith);
        end

    case 9                  % Terminate
        sys = [ ];

end
```

Fig. 5. Laser model listing.

test set presented in Fig. 6. The ultra fast laser driver was based on a dedicated integrated circuit manufactured by Maxim. The independent bias and modulation current adjustment was arranged. The laser output power was supplied, via the photodiode module, to the digital oscilloscope. The square wave laser modulation (with 90 ps rise/fall time) was applied. Modulation frequency was relatively low (in the range of few MHz) to ensure that laser steady state was reached before the beginning of each pulse. The laser bias was changed from zero to the threshold current value and modulation current was adjusted to maintain the constant optical pulse amplitude. The turn-on delay was measured as a rising edge time position difference observed for overthreshold and subthreshold laser biasing. Then, the coefficient c was chosen for the best fit between Eq. (8) and the measured data.

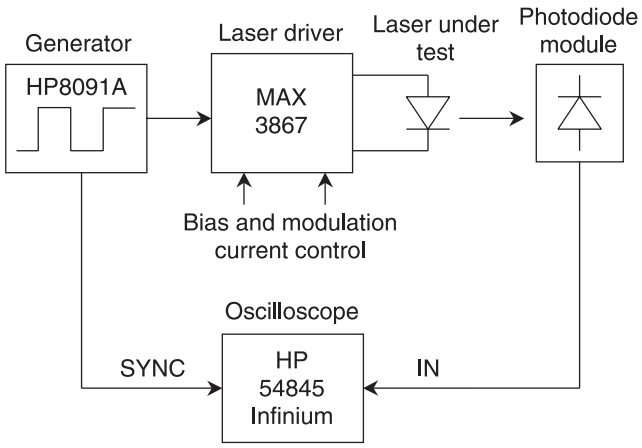

Fig. 6. Test set used for laser turn-on delay measurement.

Characterization of all measured lasers together with the obtained parameter values and estimation inaccuracies are collected in Table 1. Comparison between the measured and estimated turn-on delay plotted versus normalised bias current is illustrated in Fig. 7 for four picked lasers.

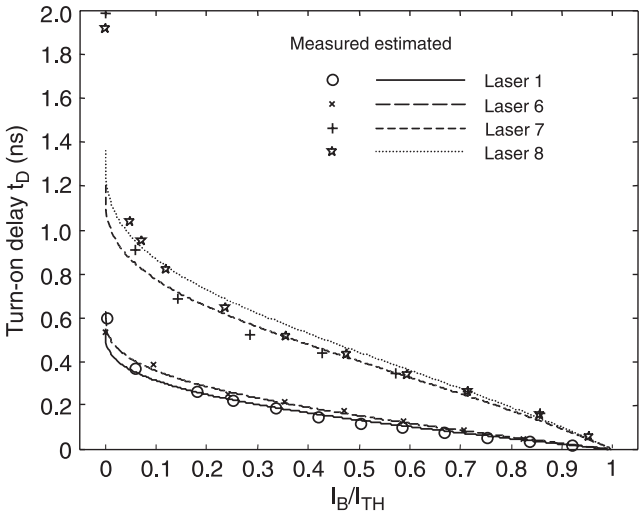

Fig. 7. Comparison between measured and estimated turn-on delay.

It can be concluded that Eqs. (6) and (8) correctly approximate the turn-on delay. The results for all measured lasers were similar. In all cases, the largest impairments was observed for zero bias current, however, the sign of this error was different from one to another device, so no *a priori* correction factor may be introduced. Omitting the data obtained for zero bias, the mean inaccuracy between estimated and measured turn-on delays was in the range of 2.6 ps (for laser No. 3) to 31 ps (for laser No. 7). It can be noticed that better approximation accuracy was obtained for nowadays MQW lasers than for bulk ones. Moreover, all measured 1.3 μm MQW lasers have similar values of c parameter what suggest that some initial analysis may be undertaken without measurement effort.

In further experiments, two of the lasers were measured at the ambient temperature, increased to 60°C. The estimated and measured turn-on delays are compared in Fig. 8. Estimation was obtained from Eq. (8) leaving the value of c extracted from previous measurements performed in normal ambient temperature. Only I_{TH} and I_F were corrected to

Table 1. Lasers characteristics.

Type	Vendor	λ (μm)	I_{TH} (mA)	Nom. power (mW)	Parameter c (ns×mA$^{2/3}$)	Estimation inaccuracy (ps)
MQW, DFB	Lucent	1.30	12.0	2.0	2.94	4.4
MQW, FP	Mitsubishi	1.30	13.0	2.0	3.01	11.2
MQW, FP	Lasermate	1.30	7.5	1.5	2.74	2.6
MQW, DFB	Lasermate	1.55	11.5	1.0	1.70	7.8
Bulk, FP	OKI	1.30	24.0	1.0	6.65	9.9
MQW, FP	AOC	1.30	8.5	1.0	2.47	5.9
Bulk, FP	AOC	1.30	35.0	1.8	4.64	31.0
Bulk, FP	AOC	1.55	42.0	1.5	6.21	27.0

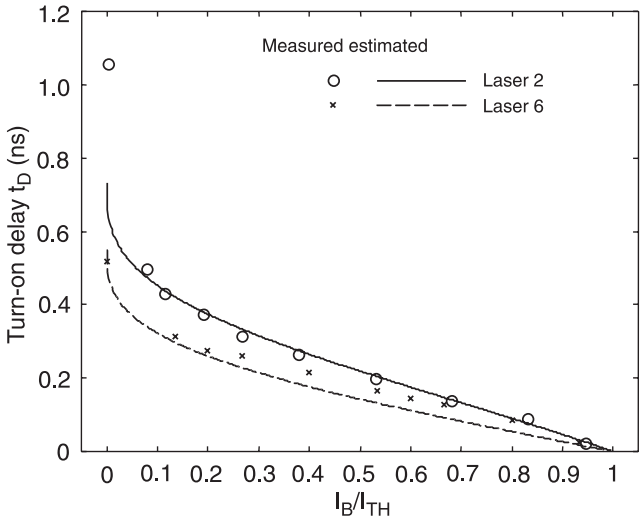

Fig. 8. Comparision between estimation and measurements performed at 60°C.

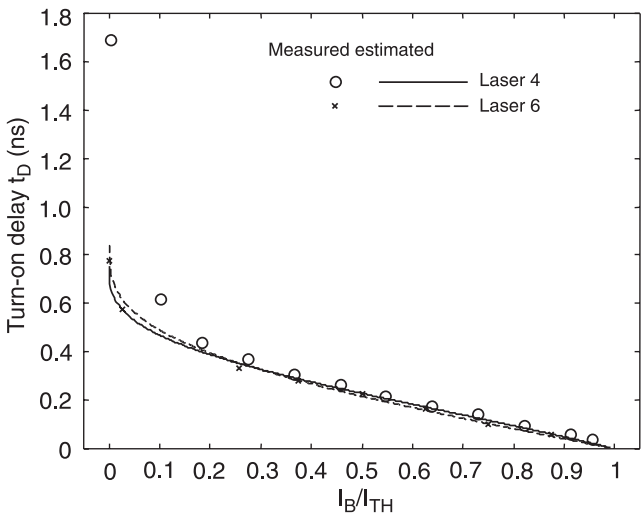

Fig. 9. Comparision between estimation and measurements performed for reduced power.

their new actual values. As it is shown, the estimation is still correct, so the parameter c seems to be practically temperature independent.

Additionally, the turn-on delay was measured with I_F reduced to obtain half of the nominal optical power from the laser. The actual value of I_F was used in Eq. (8), and the parameter c was left as extracted from previous measurements. Good agreement between measured and estimated values was obtained (Fig. 9).

Next, the data transmission eye-pattern for 1 Gb/s data rate was measured and simulated for three cases of a laser bias. The measurement set was similar to this from Fig. 6, with only the square wave generator replaced by pseudo random bit sequence (PRBS) generator. The laser used was No. 1 from Table 1. The Simulink model (Fig. 10) consisted of the laser model listed in Fig. 5, driven by PRBS generator and constant bias source. The bandwidth limitation of photodiode module (2.2 GHz) and oscilloscope (1.5 GHz) was modelled by the first order transfer functions.

The comparison between measurements and simulations are illustrated in Fig. 11. The eye degradation (rising edge jitter and horizontal eye opening reduction) is practically equal for the measured and simulated traces for all bias conditions. Some overshoots visible at the measured traces suggest that the real transfer functions of photodiode module and oscilloscope are more complicated that the first order ones, taken in simulations. However, these effects are not in the scope of our considerations.

6. Conclusions

Assuming the simplified carrier recombination description in the laser active region, the model of dynamic distortions under subthreshold bias conditions was proposed. Experimental verification of this model confirmed its usefulness in application to nowadays II and III-window communication lasers. The model allows calculating the laser turn-on delay for arbitrary bias and modulation currents. In contrast to the standard rate-equation approach, the only two easy obtainable laser parameters are needed.

Basing on the developed formulae, the simulation model prepared in Simulink was constructed to simulate dynamic data stream distortions in high-speed transmission systems. The presented model may be used to aid the design process and evaluation of high-speed laser drivers operating with subthreshold laser bias.

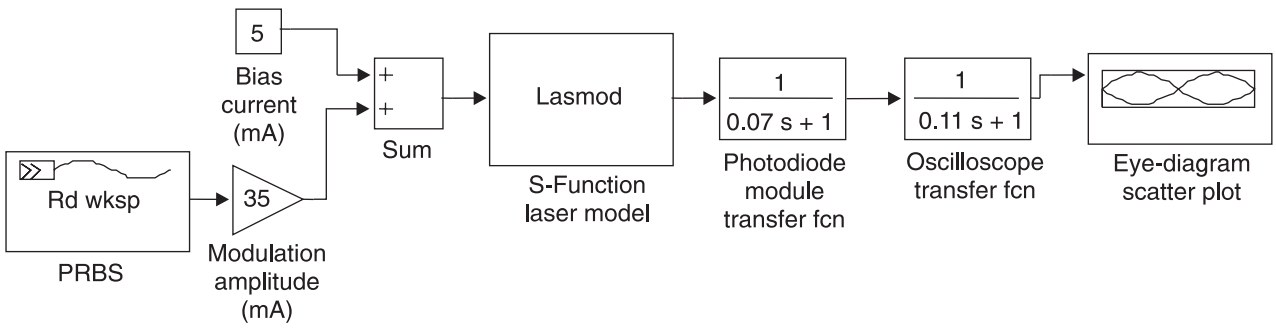

Fig. 10. Simulink model for eye pattern simulation.

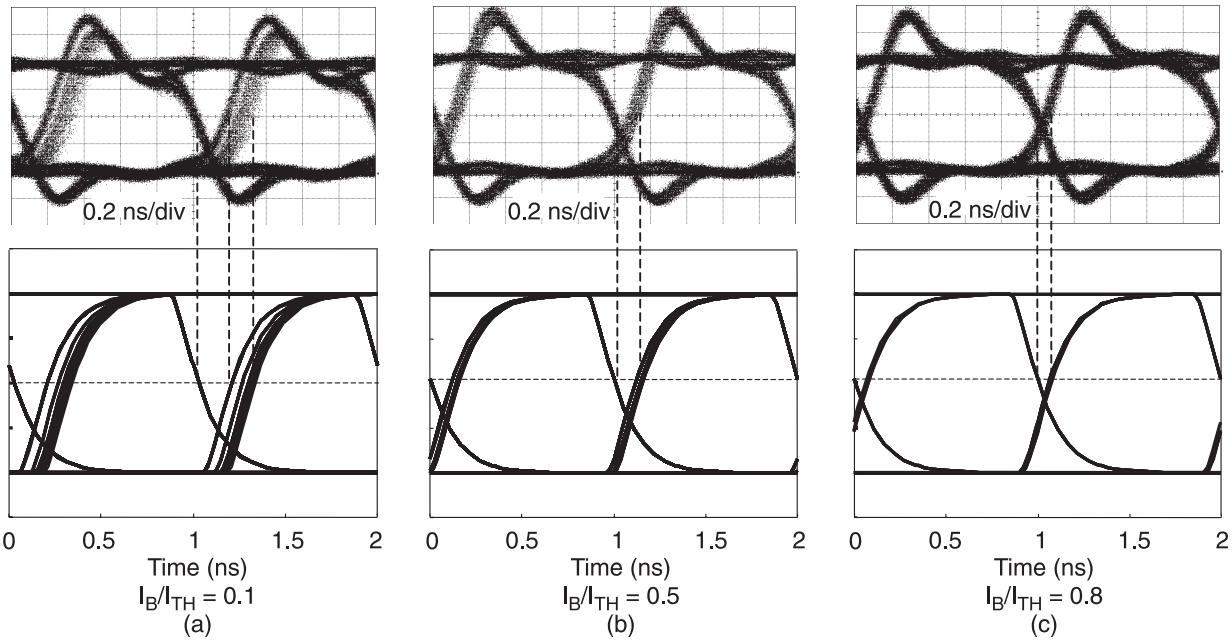

Fig. 11. Measured (upper traces) and simulated (lower traces) 1 Gb/s eye patterns.

Acknowledgements

This work was supported by the Polish State Committee for Scientific Research under the grant 4T11B05624.

References

1. G.P. Agrawal, *Fiber Optic Communication Systems*, Willey, New York, 1997.
2. N.J. Frigo, "A survey of fiber optics in local access architectures" in *Optical Fiber Telecommunications IIIA*, edited by I.P. Kaminow and T.L Koch, Academic Press, San Diego, 1997.
3. M. Yano, K. Yamaguchi, and H. Yamashita, "Global optical access systems based on ATM-PON", *FUJITSU Sci. Tech. J.* **35**, 56–70 (1999).
4. G. Kramer and G. Pesavento, "Ethernet passive optical network (EPON): building a next-generation optical access network", *IEEE Communications Magazine*, 62–73 (2002).
5. Y. Ota, R.G. Swartz, M. Tarsia, and V.D. Archer, "Low-power, high-sensitivity 30-Mbit/s burst-mode/packet receiver for PON application", OFC'94, 210–212 (1994).
6. S. Brigati, P. Colombara, L. D'Ascoli, U. Gatti, T. Kerekes, P. Malcovati, and A. Profumo, "A SiGe BiCmos burst-mode 155 Mbit/s receiver for PON", *27th European Solid State Circuit Conf.* (2001).
7. L.P. Chen, M.Y. Li, C.J. Chang-Hasnain, and K.Y. Lan: "A low-power 1 Gbit/s CMOS laser driver for a zero-bias modulated optical transmitter", *IEEE Photon. Techn. Lett.* **9**, 997–999 (1997)
8. L.A. Coldren and S.W. Corzine, *Diode Lasers and Photonic Integrated Circuits*, Wiley, New York, 1995.
9. B. Mroziewicz, M. Bugajski, and W. Nakwaski, *Physics of Semiconductor Lasers*, PWN, Warsaw, 1991.
10. G.P. Agrawal and T.M. Shen, "Power penalty due to decision-time jitter in optical communication systems", *Electron. Lett.* **22**, 718–719 (1987).
11. K. Schumacher and J.J. O'Reilly, "Power penalty due to jitter on optical communication systems", *Electron. Lett.* **23**, 450–451 (1986).
12. H.M. Salgado, M.M. Freire, and J.J. O'Reilly, "Extraction of semiconductor intrinsic laser parameters by intermodulation distortion analysis", *IEEE Photon. Techn. Letters* **9**, 1331–1333 (1997).
13. J.C. Cartledge and R.C. Srinivasan, "Extraction of DFB laser rate equation parameters for system simulation purposes", *IEEE J. Lightwave Techn.* **15**, 852–860 (1997).

